

Multifidelity Orbit Uncertainty Propagation using Taylor Polynomials

Alberto Fossà*

Institut Supérieur de l'Aéronautique et de l'Espace, Toulouse, 31055, France

Roberto Armellin†

The University of Auckland, Auckland, 1010, New Zealand

Emmanuel Delande‡

Centre National d'Études Spatiales, Toulouse, 31401, France

Matteo Losacco§

Institut Supérieur de l'Aéronautique et de l'Espace, Toulouse, 31055, France

Francesco Sanfedino¶

Institut Supérieur de l'Aéronautique et de l'Espace, Toulouse, 31055, France

A new multifidelity method is developed for nonlinear orbit uncertainty propagation. This approach guarantees improved computational efficiency and limited accuracy losses compared to fully high-fidelity counterparts. The initial uncertainty is modeled as a weighted sum of Gaussian distributions whose number is adapted online to satisfy the required accuracy. As needed, univariate splitting libraries are used to split the mixture components along the direction of maximum nonlinearity. Differential Algebraic techniques are used to propagate these Gaussian kernels and compute a measure of nonlinearity required for the split decision and direction identification. Taylor expansions of the flow of the dynamics are computed using a low-fidelity dynamical model to maximize computational efficiency and corrected with selected high-fidelity samples to minimize accuracy losses. The effectiveness of the proposed method is demonstrated for different dynamical regimes combining SGP4 theory and numerical propagation as low- and high-fidelity models respectively.

I. Introduction

ACCURATE propagation of uncertainties is key for Space Situational Awareness (SSA) applications. Ranging from Space Surveillance and Tracking (SST) to Collision Avoidance Maneuver (CAM) planning, these activities require the estimation of the spacecraft state at a future epoch given the Initial Conditions (ICs) at an earlier time. These ICs are the result of ground-based observations or on-board Orbit Determination (OD) techniques, which are stochastic in nature. The propagation of a nominal state is thus not sufficient, but it is rather required to propagate the associated initial Probability Density Function (PDF) resulting from the estimation procedure. Given the intrinsic nonlinearity of the dynamics, no analytical solution exists to map the aforementioned PDF. On the contrary, several methods exist to approximate this quantity with increasing level of accuracy, usually at the expenses of higher computational efforts. Instead, this paper focuses on a novel multifidelity approach to tackle the Uncertainty Propagation (UP) problem in orbital dynamics which guarantees a similar accuracy of high-fidelity techniques with a reduced computational load.

Previous approaches tackled the UP problem in different ways, the most widely used being linear methods and sample-based techniques [1]. Linear methods build on the assumptions that a linearized dynamical model is sufficient to capture the dynamics of neighboring trajectories and that the uncertainty can be completely characterized by a multivariate Gaussian distribution. Under these assumptions, only the mean and the covariance matrix need to be

*PhD Candidate, Department of Aerospace Vehicles Design and Control, 10 Avenue Edouard Belin.

†Professor of Astrodynamics, Te Pūnaha Ātea - Space Institute, 20 Symonds Street.

‡Space Surveillance Engineer, Space Surveillance and Tracking, 18 Avenue Edouard Belin.

§Postdoctoral Researcher, Department of Aerospace Vehicles Design and Control, 10 Avenue Edouard Belin.

¶Associate Professor, Department of Aerospace Vehicles Design and Control, 10 Avenue Edouard Belin.

propagated, and the problem reduces to the integration of the State Transition Matrix (STM) known as Linear Covariance (LinCov) propagation. However, if the dynamics is highly nonlinear, this approach fails to accurately describe the time evolution of the state PDF. An extension of the LinCov method is that of State Transition Tensors (STTs), which are higher-order Taylor expansions of the dynamics about the nominal trajectory [2]. However, this method is not ideal for complex dynamics at high orders since it requires the derivation of analytical expressions for the variational equations and their numerical integration along with the reference trajectory.

On the other side, Monte Carlo (MC) simulations are widely used in operational scenarios since they provide highly accurate estimation of the state uncertainty and are easy to implement. Yet their accuracy comes with a major computational cost, which makes MC techniques not applicable for real-time applications or maintenance of very large space objects catalogs. Sample based methods also include Unscented Transform (UT) and Conjugate Unscented Transform (CUT) [3–5], which are deterministic in nature as opposed to stochastic MC simulations. These methods are based on the idea that is easier to approximate a state PDF than an arbitrary nonlinear transformation. Assuming a Gaussian distribution for the initial state uncertainty, they enforce the corresponding Moment Constraint Equations (MCEs) up to a given order to solve for a deterministic set of samples, denoted as sigma points, whose weighted statistics correctly capture the first statistical moments of the state PDF. To reduce the search space, these points are constrained to lie on carefully selected set of axes, and a fully symmetric set is chosen to automatically satisfy the MCEs for any odd moment of the Gaussian distribution. If the UT can only capture the statistical moments up to third order, CUT sigma points sets were obtained to match these moments up to ninth order. However, this approach suffers from a rapid increase in the number of samples needed to satisfy the MCEs for increasing orders and state dimension.

Polynomial Chaos Expansion (PCE) is another samples-based technique developed for UP [6]. This method aims at obtaining a functional representation of the propagated uncertainty with respect to the input random variables, thus providing accurate information on higher-order statistical moments of the state PDF. Inputs and outputs of the considered transformation are represented by series approximations of standard random variables rewritten as series expansions of orthogonal polynomials for which the coefficients are sought. This technique requires a number of PCE terms which varies exponentially with both the order of the polynomial basis and the dimensions of the input random variables, leading to the curse of dimensionality for large problems.

A new multifidelity technique based on Taylor polynomials is developed in this work to address the need for accurate and less computationally expensive methods for nonlinear Uncertainty Propagation in orbital dynamics. In this context, multifidelity techniques combine different fidelity force models to accurately propagate the state PDF at a reduced cost [6, 7]. With sample-based methods such as PCE, this approach requires the propagation of most samples in low-fidelity dynamics and the evaluation of the high-fidelity model on few carefully chosen points to correct the initial approximate solution. On the contrary, the proposed method relies on a Taylor expansion of the low-fidelity dynamics for which only the constant part needs to be propagated with the high-fidelity model.

Taylor algebra, or Differential Algebra (DA), provides the tools to compute the arbitrary-order derivatives of a function within a computer environment [8]. In the context of UP, DA is similar to STTs in the sense that it provides an expansion of the flow of the dynamics around the nominal state in the form of a Taylor polynomial of order n . This information was successfully employed in previous work to map the initial state uncertainties through the nonlinear orbital dynamics [9, 10]. However, if the transformation under consideration is strongly nonlinear, a single Taylor polynomial might fail to accurately describe the ODE flow in the domain of interest around the nominal solution. Automatic Domain Splitting (ADS) techniques were developed to overcome this issue [11]. The idea is to continuously monitor the accuracy of the Taylor expansion by estimating the magnitude of the truncated terms (terms of order $n + 1$) and react consequently when the imposed error threshold is violated. When it happens, the single polynomial is split into two new expansions, each of them covering only half of the initial domain, so as to meet the specified accuracy. This algorithm requires an expansion order ≥ 3 and its accuracy increases for increasing orders. In this work, a novel splitting algorithm specifically developed for second-order Taylor expansions and named LOADS (Low-Order Automatic Domain Splitting) is employed instead [12].

Gaussian Mixture Models (GMMs) can approximate an arbitrary PDF using a weighted sum of Gaussian distributions, and this approximation converges to the true PDF as the number of components approaches infinity. In orbit UP, algorithms were developed to adapt online the number of GMM components required to correctly capture the entire state PDF as the assumption of Gaussianity becomes less accurate for longer propagation times or stronger nonlinearities [13]. In this scenario, the initial uncertainty is described using a single Gaussian kernel and a metric is used throughout the propagation step to continuously monitor the error between linearized and fully nonlinear models. When the specified threshold is violated, the propagation is halted to split the single kernel into components and then resumed on the newly obtained kernels. Other works [14, 15] simplify this approach by performing all required splits on the initial distribution

and keep the number of Gaussian kernels fixed for the whole propagation time span. However, compared to their adaptive counterparts, these methods suffer from an increased computational effort due to the large number of kernels to be handled in the early stages of propagation. Hybrid methods were proposed that combine GMMs with Extended Kalman Filter (EKF), Unscented Kalman Filter (UKF) [13], PCEs [15], and DA [16], but the Taylor expansions of the dynamics were never used to inform the splitting into the GMM components.

In this context, a novel multifidelity (MF) method that combines DA-based propagation and adaptive splitting of GMMs in low-fidelity (LF) dynamics with point-wise (PW) propagation of the polynomials centers in high-fidelity (HF) is presented. In the LF step, a second-order Taylor expansion of the flow is used to compute the Nonlinearity Index ν . When its magnitude crosses a given threshold, the polynomial is split into three new expansions such that the assumption of a quasi-linear transformation still holds in each subdomain. Assuming a Gaussian distribution for the initial state, the IC is constructed such that the former distribution is correctly captured within the domain of validity of its Taylor polynomial. As the propagation steps forward, more domains are generated by the LOADS algorithm, each of them corresponding to a new GMM component such that their weighted sum correctly captures the true non-Gaussian state PDF. Once the DA-based propagation has ended, evaluation of the resulting polynomials on UT sigma-points is used to map the statistics of the initial components to final time. The HF step is then simply a PW propagation of the means of these Gaussian kernels for the same time span. The resulting final states will constitute the polynomials centers and components means of the updated MF solution.

Nonlinearity of any dynamical system is not an intrinsic attribute of the system itself, but is rather coupled with the mathematical representation chosen to describe its geometry, kinematics and evolution dynamics [17]. In the context of orbit UP, this aspect is emphasized by the choice of Orbital Elements (OEs) used to describe the osculating orbit state. As a consequence, the performance of the developed LOADS-GMM algorithm is expected to be strongly affected by this choice of state parametrization, being the splitting decision derived from a measure of nonlinearity of the neighboring dynamics. If cartesian coordinates are widely used in end-user applications, their evolution over time is strongly nonlinear due to the Keplerian attraction being proportional to $1/r^2$. Several OEs sets adapted to the underlying dynamics were thus proposed to mitigate these nonlinearities. Examples include Keplerian elements, equinoctial elements [18] and Modified Equinoctial Elements [19]. Under the assumption of unperturbed Keplerian motion, five of these coordinates describe the shape and spatial orientation of the orbit and are thus constant in time, while the last provides the instantaneous position of the object along its closed path. More recently, Horwood et al. [14] introduced a set of alternate equinoctial elements which, in absence of perturbations, evolve linearly in time demonstrating their effectiveness for orbit UP using Gaussian sum filters. The hypothesis of restricted two-body dynamics was then removed by Aristoff et al. [20] who proposed a set of J_2 equinoctial orbital elements that absorb the perturbation due to the equatorial bulge of the central attracting body. Finally, Baù et al. [21] introduced the generalized equinoctial orbital elements which extend this approach to any perturbing force derived from a potential.

The paper is organized as follows. After a short description of the DA formalism in Section II, the LOADS algorithm is described in Section II.A. GMMs are then introduced in Section II.B. Section II.B.1 describes the univariate splitting libraries for standard normal distributions while Section II.B.2 discusses their extension to the multivariate case. Section II.C presents the combined LOADS-GMM algorithm for UP that constitutes the LF step of the proposed method. The MF approach is then described in Section III. Three numerical applications to the problem of orbit UP are then included in Section IV and the accuracy of the MF method compared against reference MC simulations. The importance of the HF correction and the computational efficiency of the overall method are then assessed in Sections IV.C and IV.D respectively. Conclusions are finally drawn in Section V.

II. Uncertainty Propagation

Consider the generic nonlinear transformation $f: \mathbb{R}^n \rightarrow \mathbb{R}^m$

$$\mathbf{y} = f(\mathbf{x}) \quad (1)$$

and two multivariate random variables \mathbf{X}, \mathbf{Y} defined on $\mathbb{R}^n, \mathbb{R}^m$ with PDFs p_X, p_Y respectively. The problem of nonlinear UP consists in estimating p_Y from the only knowledge of p_X and f . In DA framework, \mathbf{X} is expressed as a function of its expected value and associated uncertainty as

$$[\mathbf{x}] = \bar{\mathbf{x}} + \boldsymbol{\beta} \cdot \delta \mathbf{x} \quad (2)$$

with $\bar{\mathbf{x}} = \mathbb{E}[\mathbf{X}]$, $\boldsymbol{\beta}$ Confidence Interval (CI) semi-amplitude and $\delta \mathbf{x}$ first-order variations around $\bar{\mathbf{x}}$.

Evaluating f in the DA framework results in the Taylor expansion of y in terms of δx expressed as

$$[y] = f([y]) = \mathcal{T}_y(\delta x) \quad (3)$$

The polynomials in Eq. (3) can then be used to efficiently compute the propagated statistics as described in Section II.B.

A. Low-Order Automatic Domain Splitting

The LOADS algorithm is a DA-based method that aims at solving the uncertainty propagation problem by splitting the uncertainty set into a manifold of second-order Taylor expansions [12]. The splitting decision and direction are determined by a proper measure of nonlinearity that is derived from the analysis of the Taylor expansion of the Jacobian of the transformation. This Nonlinearity Index (NLI) ν is a reformulation in DA sense of the same parameter introduced by Junkins and Singla [17] and approximates the relative error between full nonlinear and linearized transformations at the edges of the domains on which the Taylor polynomials are defined.

Consider the generic transformation f and a second order expansion for $[x]$. The Jacobian of f is defined as the $m \times n$ matrix $[J]$ of the partials of f with respect to $[x]$

$$[J_{ij}] = \frac{\partial f_i}{\partial x_j} \quad i = 1, \dots, m \quad j = 1, \dots, n \quad (4)$$

If the transformation is linear, the Taylor expansion of the Jacobian coincides with its constant part, i.e. $[J] = \bar{J}$. On the contrary, if the transformation is nonlinear, each component $[J_{ij}]$ of $[J]$ is a first-order Taylor expansion in the deviations δx , i.e.

$$[J_{ij}] = \bar{J}_{ij} + \delta J_{ij} = \mathcal{T}_{J_{ij}}(\delta x) \quad (5)$$

Consider now the non-constant part of the Jacobian matrix elements, δJ_{ij} . Each element can be expressed as a linear combination of the variables δx_k for $k = 1, \dots, n$, i.e.

$$\delta J_{ij} = \mathcal{T}_{\delta J_{ij}} = \sum_{k=1}^n a_{ij,k} \delta x_k \quad (6)$$

as a result, a rigorous estimation of the variation range of each term δJ_{ij} can be obtained as

$$b_{\delta J_{ij}} = \sum_{k=1}^n |a_{ij,k}| \quad (7)$$

$$\delta J_{ij} \in [-b_{\delta J_{ij}}, b_{\delta J_{ij}}]$$

The idea behind the LOADS algorithm is to use these bounds as a measure of nonlinearity of the transformation. More specifically, the NLI is expressed as

$$\nu = \frac{\sum_{i=1}^m \sum_{j=1}^n b_{\delta J_{ij}}}{\sum_{i=1}^m \sum_{j=1}^n |\bar{J}_{ij}|} = \frac{\sum_{i=1}^m \sum_{j=1}^n \sum_{k=1}^n |a_{ij,k}|}{\sum_{i=1}^m \sum_{j=1}^n |\bar{J}_{ij}|} \quad (8)$$

Therefore, the index ν is obtained as the ratio between the entry-wise 1-norm of the matrix of the bounds and the entry-wise 1-norm of the constant part of the Jacobian. In case of linear transformation, all elements $b_{\delta J_{ij}}$ are identically equal to zero, so $\nu = 0$. As the transformation departs from linearity, the numerator increases, thus a hint on the nonlinear nature of the investigated problem is obtained.

In case nonlinearities are detected, the algorithm proceeds by splitting the uncertainty set along a determined direction k . The identification of the splitting direction is done with the same procedure. The only element that changes is the processed Jacobian. More specifically, given an investigated splitting direction e and the associated variable δx_e , defining as δx_e the vector

$$\delta x_e = \{0, \dots, 0, \delta x_e, 0, \dots, 0\}^T \quad e \in [1, \dots, n] \quad (9)$$

a directional Jacobian is built as the composition of $[\mathbf{J}(\delta\mathbf{x})]$ with $\delta\mathbf{x}_e$, i.e.

$$[\mathbf{J}|_e] = \mathcal{T}_{\mathbf{J}}(\delta\mathbf{x}) \circ \delta\mathbf{x}_e = \mathcal{T}_{\mathbf{J}|_e}(\delta\mathbf{x}_e) \quad (10)$$

The directional NLI is then computed as

$$v_e = \frac{\sum_{i=1}^m \sum_{j=1}^n b_{\delta J_{ij}|_e}}{\sum_{i=1}^m \sum_{j=1}^n |\bar{J}_{ij}|} \quad (11)$$

The splitting direction k is finally selected as the one corresponding to the maximum directional index, i.e.

$$k = \arg \max_e \{v_e\} \quad (12)$$

Once the splitting direction has been determined, the current set $[\mathbf{x}]$ is split according to the preselected splitting library \mathcal{S}_l as described in Section II.C, thus generating a list of N_{sub} subsets $[\mathbf{x}^{(p)}]$ with N_{sub} size of the library itself.

The splitting algorithm is then embedded in an iterative procedure as described in Algorithm 1 to generate the so-called manifold M_y of subdomains $[\mathbf{y}^{(p)}]$ that satisfy the imposed constraints. These constraints include a maximum nonlinearity threshold ε_v and a maximum number of splits N_{max} so that $v^{(p)} < \varepsilon_v \vee N_{splits}^{(p)} = N_{max} \forall [\mathbf{y}^{(p)}] \in M_y$. The choice of $\varepsilon_v \in \mathbb{R}^+$ is thus a trade-off between accuracy of the DA maps, increasing for $\varepsilon_v \rightarrow 0$, and size of the output manifold M_y , decreasing for $\varepsilon_v \rightarrow +\infty$. However, being v a direct measure of the relative error between full nonlinear and linearized transformations, ε_v must be chosen sufficiently small ($\varepsilon_v \ll 1$) to guarantee an acceptable accuracy of the output DA maps. A more exhaustive analysis of Algorithm 1 can be found in [12] where the LOADS algorithm is applied to the investigated case of orbit UP, and a detailed analysis of the role played by the different control parameters is offered.

Algorithm 1 LOADS algorithm

function LOADS($f, [\mathbf{x}], \varepsilon_v, N_{max}, \mathcal{S}_l$)

Initialize the working and output manifolds W_x, M_x, M_y

Add $[\mathbf{x}]$ to W_x

while W_x is not empty **do**

Remove the first set $[\mathbf{x}^{(p)}]$ from W_x

Evaluate $[\mathbf{y}^{(p)}] = f([\mathbf{x}^{(p)}])$

Compute the NLI $v^{(p)}$

▷ see Eqs. (4) to (8)

if $v^{(p)} < \varepsilon_v \vee N_{splits}^{(p)} = N_{max}$ **then**

Add $[\mathbf{x}^{(p)}]$ to M_x and $[\mathbf{y}^{(p)}]$ to M_y

else

Compute the splitting direction k

▷ see Eqs. (10) to (12)

Split $[\mathbf{x}^{(p)}]$ into $[\mathbf{x}^{(i)}]$ for $i = 1, \dots, N_{sub}$

▷ see Section II.C

Add all $[\mathbf{x}^{(i)}]$ to W_x

end if

end while

return M_x, M_y

B. Gaussian Mixture Model

Consider a multivariate random variable \mathbf{X} defined on \mathbb{R}^n with PDF $p_{\mathbf{X}}$. The probability density function $p_{\mathbf{X}}$ has no general closed-form solution and might be approximated using different techniques. However, if \mathbf{X} is Gaussian with mean $\boldsymbol{\mu}_{\mathbf{X}} \in \mathbb{R}^n$ and covariance $\mathbf{P}_{\mathbf{X}} \in \mathbb{R}^{n \times n}$, its PDF has the well-known analytical expression

$$p_{\mathbf{X}}(\mathbf{x}) = \mathcal{N}(\mathbf{x}; \boldsymbol{\mu}_{\mathbf{X}}, \mathbf{P}_{\mathbf{X}}) = \frac{1}{\sqrt{|2\pi\mathbf{P}_{\mathbf{X}}|}} \cdot \exp\left\{-\frac{1}{2}(\mathbf{x} - \boldsymbol{\mu}_{\mathbf{X}})^T \mathbf{P}_{\mathbf{X}}^{-1}(\mathbf{x} - \boldsymbol{\mu}_{\mathbf{X}})\right\} \quad (13)$$

where $|\cdot|$ represents the matrix determinant.

GMMs leverage this property to obtain analytic approximations of arbitrary PDFs as weighted sums of Gaussian distributions. For a generic random variable \mathbf{X} , its PDF is thus expressed as

$$p_{\mathbf{X}}(\mathbf{x}) \simeq \sum_{i=1}^L \alpha_i p_{\mathcal{N}}(\mathbf{x}; \boldsymbol{\mu}_i, \mathbf{P}_i) \quad (14)$$

with L total number of components and α_i mixing proportions or weights subject to

$$\alpha_i \geq 0 \quad \forall i \in \{1, \dots, L\} \quad (15a)$$

$$\sum_{i=1}^L \alpha_i = 1 \quad (15b)$$

If \mathbf{X} is subject to a nonlinear transformation such as Eq. (1), the number of components L that guarantees an accurate representation of the input PDF $p_{\mathbf{X}}$ might fail to correctly capture the shape of the transformed PDF $p_{\mathbf{Y}}$. A splitting algorithm is thus employed to dynamically adapt this number so that $p_{\mathbf{Y}}$ is approximated with the desired accuracy. Its formulation is described in Sections II.B.1, II.B.2 and II.C.

1. Univariate Splitting Library

Consider the univariate standard Gaussian distribution $X \sim \mathcal{N}(0, 1)$ with PDF

$$p_X(x) = p_{\mathcal{N}}(x; 0, 1) \quad (16)$$

for the purpose of computing a univariate splitting library, it is desired to approximate Eq. (16) with a GMM such that

$$p_X(x) \simeq \sum_{i=0}^{L-1} \tilde{\alpha}_i p_{\mathcal{N}}(x; \tilde{\mu}_i, \tilde{\sigma}_i^2) \quad (17)$$

with L number of components and $\tilde{\alpha}_i, \tilde{\mu}_i, \tilde{\sigma}_i^2$ mixture weights, means and variances respectively. After selecting the number of components L , a minimization problem is formulated to determine the remaining $3L$ parameters. The number of free variables can be then further reduced constraining the GMM to be homoscedastic, i.e.

$$\tilde{\sigma}_i^2 = \tilde{\sigma}^2 \quad \forall i \in \{0, \dots, L-1\} \quad (18)$$

and taking advantage of the symmetric shape of p_X about the mean. Equation (17) is thus rewritten as

$$p_X(x) \simeq \tilde{\alpha}_0 \cdot p_{\mathcal{N}}(x; 0, \tilde{\sigma}^2) + \sum_{i=1}^l \tilde{\alpha}_i \cdot \left[p_{\mathcal{N}}(x; -\tilde{\mu}_i, \tilde{\sigma}^2) + p_{\mathcal{N}}(x; \tilde{\mu}_i, \tilde{\sigma}^2) \right] \quad (19)$$

with $l = \lfloor L/2 \rfloor$ and $\alpha_0 = 0$ if L is even so that only $L+1$ parameters remain to be determined.

To solve for the optimal $\tilde{\alpha}_i, \tilde{\mu}_i$ and $\tilde{\sigma}^2$ a performance index J is developed starting from the L_2 distance between PDFs defined as

$$L_2(p_1, p_2) = \int_{\mathbb{R}^n} [p_1(\mathbf{x}) - p_2(\mathbf{x})]^2 d\mathbf{x} \quad (20)$$

The L_2 distance is preferred here instead of other measures since an analytical expression for Eq. (20) exists if both p_1, p_2 are approximated by GMMs as

$$p_1(\mathbf{x}) \simeq \sum_{i=1}^{L_1} \alpha_{1,i} p_{\mathcal{N}}(\mathbf{x}; \boldsymbol{\mu}_{1,i}, \mathbf{P}_{1,i}) \quad (21a)$$

$$p_2(\mathbf{x}) \simeq \sum_{j=1}^{L_2} \alpha_{2,j} p_{\mathcal{N}}(\mathbf{x}; \boldsymbol{\mu}_{2,j}, \mathbf{P}_{2,j}) \quad (21b)$$

substituting Eq. (21) into Eq. (20) leads in fact to the following expression for L_2

$$L_2(p_1, p_2) = d_{1,1} + d_{2,2} - 2 \cdot d_{1,2} \quad (22)$$

with

$$d_{m,n} = \sum_{i=1}^{L_m} \sum_{j=1}^{L_n} \alpha_{m,i} \alpha_{n,j} K(\boldsymbol{\mu}_{m,i}, \boldsymbol{\mu}_{n,j}, \mathbf{P}_{m,i} + \mathbf{P}_{n,j}) \quad m, n = 1, 2 \quad (23)$$

and K defined as

$$K(\boldsymbol{\mu}_1, \boldsymbol{\mu}_2, \mathbf{P}_1 + \mathbf{P}_2) = \frac{1}{\sqrt{|2\pi(\mathbf{P}_1 + \mathbf{P}_2)|}} \cdot \exp\left\{-\frac{1}{2}(\boldsymbol{\mu}_1 - \boldsymbol{\mu}_2)^T (\mathbf{P}_1 + \mathbf{P}_2)^{-1} (\boldsymbol{\mu}_1 - \boldsymbol{\mu}_2)\right\} \quad (24)$$

After setting $p_1 = p = p_{\mathcal{N}}(x; 0, 1)$ and $p_2 = \tilde{p}$ equal to the RHS of Eq. (19), Eq. (22) further simplifies into

$$\begin{aligned} L_2(p, \tilde{p}) &= \frac{1}{2\sqrt{\pi}} - \frac{2\tilde{\alpha}_0}{\sqrt{2\pi(1 + \tilde{\sigma}^2)}} \\ &+ \frac{1}{2\sqrt{\pi\tilde{\sigma}^2}} \left[\tilde{\alpha}_0^2 + 4\tilde{\alpha}_0 \sum_{i=1}^l \tilde{\alpha}_i \exp\left\{-\frac{\tilde{\mu}_i^2}{4\tilde{\sigma}^2}\right\} \right] \\ &+ \frac{1}{\sqrt{\pi\tilde{\sigma}^2}} \sum_{i=1}^l \sum_{j=1}^l \tilde{\alpha}_i \tilde{\alpha}_j \left[\exp\left\{-\frac{(\tilde{\mu}_i - \tilde{\mu}_j)^2}{4\tilde{\sigma}^2}\right\} + \exp\left\{-\frac{(\tilde{\mu}_i + \tilde{\mu}_j)^2}{4\tilde{\sigma}^2}\right\} \right] \\ &- \frac{4}{\sqrt{2\pi(1 + \tilde{\sigma}^2)}} \sum_{i=1}^l \tilde{\alpha}_i \exp\left\{-\frac{\tilde{\mu}_i^2}{2(1 + \tilde{\sigma}^2)}\right\} \end{aligned} \quad (25)$$

The nonlinear optimization problem is finally stated as follows.

Minimize

$$J = L_2(p, \tilde{p}) + \lambda \tilde{\sigma}^2 \quad (26)$$

subject to the single equality constraint

$$0 = 1 - \tilde{\alpha}_0 - 2 \sum_{i=1}^l \tilde{\alpha}_i \quad (27)$$

and inequality constraints

$$0 < \tilde{\alpha}_i < \tilde{\alpha}_{i-1} \quad i = 2, \dots, l \quad (28a)$$

$$0 < \tilde{\mu}_{i-1} < \tilde{\mu}_i \quad i = 2, \dots, l \quad (28b)$$

where $\lambda > 0$ is a penalty factor that scales the importance of minimizing $\tilde{\sigma}^2$ with respect to $L_2(p, \tilde{p})$. Selecting $\lambda \rightarrow 0$ results in less uniform weights $\tilde{\alpha}_i$ with the largest ones allocated to the central kernels, components means $\tilde{\mu}_i$ closer to zero and a larger variance $\tilde{\sigma}^2$. The corresponding splitting libraries will then lead to an higher number of splits when

employed by the LOADS algorithm. On the contrary, choosing $\lambda \rightarrow 1$ results in more equally distributed weights, farther means and a smaller variance, thus reducing the required number of splits.

After selecting a value for λ , the Nonlinear Programming Problem (NLP) resulting from Eqs. (26) to (28) is solved numerically using the interior point optimizer IPOPT [22] compiled against the HSL Mathematical Software Library for the solution of sparse linear systems [23]. The optimal solution for $L = 3$ and $\lambda = 10^{-3}$ is given in Table 1.

i	$\tilde{\alpha}_i$	$\tilde{\mu}_i$	$\tilde{\sigma}$
1	0.2252246852539708	-1.0575150485760967	0.6715664864669252
2	0.5495506294920584	0.0	0.6715664864669252
3	0.2252246852539708	1.0575150485760967	0.6715664864669252

Table 1 Univariate splitting library for $L = 3$ and $\lambda = 10^{-3}$

2. Splitting Multivariate Distributions

Gaussian distributions remain Gaussian under linear transformations. Moreover, if \mathbf{X} is Gaussian-distributed, then the support of its PDF is the whole state space \mathbb{R}^n . However, for practical purposes, the support can be considered zero outside a CI around the mean value $\boldsymbol{\mu}_{\mathbf{X}}$. For univariate Gaussian distributions, a typical value for its semi-amplitude is that of 3σ which accounts for $\approx 99.7\%$ of all realizations. Its PDF may thus be rescaled so as to be zero beyond three standard deviations from its mean. This concept is extended to multivariate PDFs by introducing a multivariate splitting procedure that adaptively increases the number of components in Eq. (14) and reduces their covariance matrices \mathbf{P}_i so that the assumption of a linear transformation holds in the neighborhood of $\boldsymbol{\mu}_i$ in which $p_{\mathcal{N}}(\mathbf{x}; \boldsymbol{\mu}_i, \mathbf{P}_i)$ is considered to be nonzero. This condition must be verified separately for each component i and direction k thus resulting in the recursive algorithm described below.

Given a single Gaussian kernel $p_{\mathcal{N}}(\mathbf{x}; \boldsymbol{\mu}_i, \mathbf{P}_i)$ with weight α_i for which a split is deemed necessary, a univariate splitting library is used to perform this operation in the direction defined by the k^{th} eigenvector of \mathbf{P}_i [13]. In this work, the splitting direction k is determined by the LOADS algorithm described in Section II.A. Moreover, the univariate splitting library is computed offline and reused as many time as necessary during the splitting procedure.

Without loss of generality, consider a single kernel of Eq. (14) with weight, mean and covariance $\alpha, \boldsymbol{\mu}, \mathbf{P}$ respectively. The spectral factorization of \mathbf{P} is then obtained as

$$\mathbf{P} = \mathbf{V}\boldsymbol{\Lambda}\mathbf{V}^T \quad (29)$$

where \mathbf{V} is an orthogonal matrix of right eigenvectors of \mathbf{P} and $\boldsymbol{\Lambda}$ a diagonal matrix of corresponding eigenvalues. Performing the split along the k^{th} axis of the spectral factorization results in the following weights, means and covariance for the L new GMM components

$$\alpha_i = \tilde{\alpha}_i \alpha \quad (30a)$$

$$\boldsymbol{\mu}_i = \boldsymbol{\mu} + \sqrt{\lambda_k} \tilde{\mu}_i \mathbf{v}_k \quad (30b)$$

$$\mathbf{P}_i = \mathbf{V}\boldsymbol{\Lambda}_i\mathbf{V}^T \quad (30c)$$

with \mathbf{v}_k k^{th} column of \mathbf{V} , λ_k corresponding eigenvalue and $\boldsymbol{\Lambda}_i$ defined as

$$\boldsymbol{\Lambda}_i = \begin{bmatrix} \lambda_1 & & & & \\ & \dots & & & \\ & & \tilde{\sigma}^2 \lambda_k & & \\ & & & \dots & \\ & & & & \lambda_n \end{bmatrix} \quad (31)$$

3. Likelihood Agreement Measure between Distributions

The Likelihood Agreement Measure (LAM) is introduced as a measure for the accuracy of the GMM representation of the transformed PDF. Given two multivariate PDFs, the LAM is defined as [13]

$$\mathcal{L}(p, q) = \int_{\mathbb{R}^n} p(\mathbf{x})q(\mathbf{x})d\mathbf{x} \quad (32)$$

and describes the amount of overlap between the two distributions, being larger for p, q in greater agreement between each other.

If the agreement of a GMM with respect to samples resulting from a MC simulation is of interest, Eq. (32) can be reformulated treating the MC samples as a Dirac Mixture Model (DMM) as

$$\mathcal{L}(p, q) = \sum_{i=1}^{N_s} \sum_{j=1}^L \gamma_i \alpha_j p_{\mathcal{N}}(\mathbf{x}_i; \boldsymbol{\mu}_j, \mathbf{P}_j) \quad (33)$$

with N_s, L number of MC samples and Gaussian kernels respectively. Moreover, $\alpha_j, \boldsymbol{\mu}_j, \mathbf{P}_j$ are the GMM components weights, means and covariances while $\mathbf{x}_i, \gamma_i = 1/N_s \forall i$ are the propagated random samples and corresponding weights.

C. Combined LOADS-GMM algorithm

In this work, a univariate splitting library such as the one in Table 1 is embedded within the LOADS framework and the NLIs ν, ν_e defined in Eqs. (8) and (11) are used to identify the need for new splits and the corresponding directions. Moreover, an additional constraint is taken into account to bound the components weights, i.e. $\alpha^{(p)} \geq \alpha_{min} \forall p$. Given the nonlinear transformation in Eq. (1), the developed algorithm is as follows.

Firstly, the initial uncertainty on the function input \mathbf{x} is modeled with a multivariate Gaussian distribution with known mean $\boldsymbol{\mu}_0$ and covariance \mathbf{P}_0 . A CI c is then chosen and the input DA state is initialized as

$$[\mathbf{x}] = \boldsymbol{\mu}_0 + \mathbf{V}_0 \cdot \left\{ c\sqrt{\boldsymbol{\lambda}_0} \cdot \delta\mathbf{x} \right\} = \bar{\mathbf{x}}_0 + \boldsymbol{\beta}_0 \cdot \delta\mathbf{x} \quad (34)$$

where $\boldsymbol{\lambda}_0, \mathbf{V}_0$ are the eigenvalues and eigenvectors of \mathbf{P}_0 such that $\mathbf{P}_0 = \mathbf{V}_0\boldsymbol{\Lambda}_0\mathbf{V}_0^T$ with $\boldsymbol{\Lambda}_0 = \text{diag}(\boldsymbol{\lambda}_0)$. A single GMM component with $\alpha = 1, \boldsymbol{\mu}_0, \mathbf{P}_0$ is then associated to $[\mathbf{x}]$.

Secondly, a univariate splitting library \mathcal{S}_l is selected and the steps of the iterative LOADS algorithm described in Section II.A reformulated as in Algorithm 2.

Algorithm 2 Combined LOADS-GMM algorithm

function LOADSGMM($f, [\mathbf{x}], \alpha_0, \boldsymbol{\mu}_0, \mathbf{P}_0, \alpha_{min}, \varepsilon_v, N_{max}, \mathcal{S}_l$)

 Initialize the working and output manifolds W_x, M_x, M_y

 Add $[\mathbf{x}]$ to W_x
while W_x is not empty **do**

 Remove the first set $[\mathbf{x}^{(p)}]$ from W_x

 Evaluate $[\mathbf{y}^{(p)}] = f([\mathbf{x}^{(p)}])$
if $\alpha^{(p)} < \alpha_{min}$ **then**

 Add $[\mathbf{x}^{(p)}]$ to M_x and $[\mathbf{y}^{(p)}]$ to M_y
else

 Compute the scaled Jacobian $[\mathbf{J}^{(p)}]$

$$[J_{ij}^{(p)}] = \frac{1}{c\sqrt{\lambda_j^{(p)}}} \cdot \frac{\partial f_i}{\partial x_j} \quad i = 1, \dots, m \quad j = 1, \dots, n \quad (35)$$

 Compute the NLI $\nu^{(p)}$

▶ see Eqs. (5) to (8) and (35)

if $\nu^{(p)} < \varepsilon_v \vee N_{splits}^{(p)} = N_{max}$ **then**

 Add $[\mathbf{x}^{(p)}]$ to M_x and $[\mathbf{y}^{(p)}]$ to M_y
else

 Compute the splitting direction k

▶ see Eqs. (10) to (12) and (35)

 Split $[\mathbf{x}^{(p)}]$ into $[\mathbf{x}^{(i)}]$ for $i = 1, \dots, L$

$$[\mathbf{x}^{(i)}] = [\mathbf{x}^{(p)}] \circ \left\{ 0, \dots, \frac{\tilde{\mu}_i}{L} + \tilde{\sigma} \delta x_k, \dots, 0 \right\}^T \quad (36)$$

 Split $(\alpha^{(p)}, \boldsymbol{\mu}^{(p)}, \mathbf{P}^{(p)})$ into $(\alpha^{(i)}, \boldsymbol{\mu}^{(i)}, \mathbf{P}^{(i)})$ for $i = 1, \dots, L$

▶ see Eq. (30)

$$\alpha^{(i)} = \tilde{\alpha}_i \alpha^{(p)} \quad (37a)$$

$$\boldsymbol{\mu}^{(i)} = \boldsymbol{\mu}^{(p)} + \sqrt{\lambda_k^{(p)}} \tilde{\mu}_i \mathbf{v}_k^{(p)} \quad (37b)$$

$$\mathbf{P}^{(i)} = \mathbf{V}^{(p)} \boldsymbol{\Lambda}_i^{(p)} \mathbf{V}^{(p),T} \quad (37c)$$

 Add all $[\mathbf{x}^{(i)}]$ and $(\alpha^{(i)}, \boldsymbol{\mu}^{(i)}, \mathbf{P}^{(i)})$ to W_x
end if
end if
end while
return M_x, M_y

Once Algorithm 2 has converged, the PDF of the initial random variable $\mathbf{X} \sim \mathcal{N}(\boldsymbol{\mu}_0, \mathbf{P}_0)$ is approximated by a multivariate GMM whose components weights, means and covariances are stored in M_x , namely

$$p_{\mathbf{X}}(\mathbf{x}) \simeq \sum_{p=1}^P \alpha^{(p)} p_{\mathcal{N}}(\mathbf{x}; \boldsymbol{\mu}^{(p)}, \mathbf{P}^{(p)}) \quad (38)$$

with P dimension of M_x, M_y . One more step is thus needed to estimate $p_{\mathbf{Y}}$ as described in Section II.C.1.

1. Estimating GMM PDFs

Outputs of the LOADS-GMM algorithm described above comprise the GMM approximation of the initial PDF given by Eq. (38) and the Taylor expansions of the function image $[\mathbf{y}^{(p)}] = \mathbf{f}([\mathbf{x}^{(p)}])$ stored in M_y . The transformed PDF p_Y is then estimated as follows.

Firstly, a sampling scheme is chosen to draw samples from each component of the initial distribution in Eq. (38). Several sampling schemes such as Monte Carlo (MC), Unscented Transform (UT) [3] and Conjugate Unscented Transform (CUT) [5] might be employed. In this work, the UT scheme is selected since it minimizes the number sigma points while guaranteeing an exact representation of the first two statistical moments of the reconstructed PDF. This choice is deemed consistent with the second-order Taylor expansions available for $[\mathbf{y}^{(p)}]$. Following similar arguments, CUT4 and CUT6 schemes should be preferred when higher-order expansions are instead available in M_y . It was also verified that MC sampling does not provide any significant improvement in the accuracy of the estimated PDF with respect to the selected UT scheme.

Secondly, each GMM component is sampled according to its mean $\boldsymbol{\mu}^{(p)}$ and covariance $\mathbf{P}^{(p)}$. The drawn samples are then mapped through \mathbf{f} evaluating the corresponding Taylor expansion of the output $[\mathbf{y}^{(p)}] = \mathbf{f}([\mathbf{x}^{(p)}])$ stored in M_y . The first two moments of the transformed PDF are then obtained from the transformed samples as

$$\boldsymbol{\mu}_Y^{(p)} = \frac{1}{N_s} \sum_{s=1}^{N_s} \mathbf{y}_s^{(p)} \quad (39a)$$

$$\mathbf{P}_Y^{(p)} = \frac{1}{N_s - 1} \sum_{s=1}^{N_s} (\mathbf{y}_s^{(p)} - \boldsymbol{\mu}^{(p)}) (\mathbf{y}_s^{(p)} - \boldsymbol{\mu}^{(p)})^T \quad (39b)$$

for MC samples and

$$\boldsymbol{\mu}_Y^{(p)} = \sum_{s=1}^{N_s} w_s \mathbf{y}_s^{(p)} \quad (40a)$$

$$\mathbf{P}_Y^{(p)} = \sum_{s=1}^{N_s} w_s (\mathbf{y}_s^{(p)} - \boldsymbol{\mu}^{(p)}) (\mathbf{y}_s^{(p)} - \boldsymbol{\mu}^{(p)})^T \quad (40b)$$

for UT and CUT points. Here N_s is the total number of samples and w_s the associated weights with $\sum_{s=1}^{N_s} w_s = 1$.

The transformed PDF is finally estimated as

$$p_Y(\mathbf{y}) \approx \sum_{p=1}^P \alpha^{(p)} p_N(\mathbf{y}; \boldsymbol{\mu}^{(p)}, \mathbf{P}^{(p)}) \quad (41)$$

with $\boldsymbol{\mu}_Y^{(p)}, \mathbf{P}_Y^{(p)}$ given by Eq. (39) or Eq. (40).

III. Multifidelity Orbit Uncertainty Propagation

The combined LOADS-GMM algorithm presented in Section II.C can be applied to any nonlinear transformation \mathbf{f} . In the followings, its application within a multifidelity (MF) method for UP in orbital dynamics is presented. The different Orbital Elements (OEs) used to describe the orbit state are firstly introduced in Section III.A followed by a description of the DA-based Simplified General Perturbations (SGP) dynamical model and the formulation of the multifidelity LOADS-GMM algorithm in Sections III.B and III.C respectively.

A. Orbital Elements

Four Orbital Elements (OEs) sets are introduced in this section. Following the work of Junkins and Singla [17], their impact on the overall performance of the proposed multifidelity UP method is assessed in Section IV.

1. Cartesian Parameters

Cartesian parameters describe the spacecraft position and velocity in three-dimensional Euclidean space, i.e. $\mathbf{x} = [\mathbf{r} \ \dot{\mathbf{r}}]^T = [x \ y \ z \ \dot{x} \ \dot{y} \ \dot{z}]^T$. These parameters are well suited to describe third-body perturbations and nonconservative forces (SRP, atmospheric drag) acting on the spacecraft and they are commonly used in space surveillance for collision risk assessment. Under perturbed Keplerian dynamics, their evolution over time is governed by the second-order ODE

$$\ddot{\mathbf{r}} = -\frac{\mu}{r^3}\mathbf{r} + \mathbf{a}_p(\mathbf{r}, \dot{\mathbf{r}}, t) \quad (42)$$

with μ central body standard gravitational parameter, $r = \|\mathbf{r}\|_2$ and \mathbf{a}_p sum of all perturbing accelerations other than two-body central attraction. Eq. (42) is strongly nonlinear in the cartesian parameters due to the Keplerian attraction being proportional to $1/r^2$. Departure from Gaussianity will thus be magnified by the choice of this particular coordinates set resulting in a larger number of Gaussian kernels required to capture the true state PDF.

2. Equinoctial Orbital Elements

Equinoctial OEs were introduced by Broucke and Cefola [18] as an alternative to the well known Keplerian parameters to overcome some issues intrinsic of the classical set, namely a singularity for circular and/or equatorial orbits for which the Argument of Periapsis and/or the line of nodes is not defined. These new elements are expressed in terms of the Keplerian ones as*

$$\begin{aligned} a &= a \\ f &= e \cos(\omega + \Omega) \\ g &= e \sin(\omega + \Omega) \\ h &= \tan\left(\frac{i}{2}\right) \cos(\Omega) \\ k &= \tan\left(\frac{i}{2}\right) \sin(\Omega) \\ \lambda_0 &= \Omega + \omega + M_0 \end{aligned} \quad (43)$$

with a semimajor axis, e eccentricity, i inclination, Ω Right Ascension of the Ascending Node (RAAN), ω Argument of Periapsis (AOP) and M_0 mean anomaly. In this work, the mean longitude λ or true longitude L are used instead of λ_0 . They are defined as

$$\begin{aligned} \lambda &= \Omega + \omega + M \\ L &= \Omega + \omega + \nu \end{aligned} \quad (44)$$

with M, ν mean and true anomalies respectively[†].

The set of OEs in Eq. (43) is nonsingular except for retrograde equatorial orbits ($i = \pi$) and is well suited for the numerical propagation of perturbed Keplerian dynamics. Yet its application is limited to elliptic orbits ($e < 1$) with positive semimajor axis ($a > 0$). Gauss planetary equations are used throughout this paper to numerically propagate orbit states expressed in equinoctial OEs [24].

3. Modified Equinoctial Elements

Modified Equinoctial Elements (MEEs) were firstly proposed by Walker et al. [19] as an OEs set suitable for perturbation analysis of all kind of orbits. The only difference with respect to equinoctial OEs is the substitution of the semimajor axis a by the semilatus rectum $p = a(1 - e^2)$ and the mean longitude at epoch λ_0 by the true longitude L given by Eq. (44). The remaining four elements are f, g, h, k defined in Eq. (43).

MEEs are applicable to all type of orbits (elliptic, parabolic, hyperbolic) excluding retrograde equatorial ones ($i = \pi$) for which they also exhibit a singularity. These elements are particularly suitable to describe optimal control problems arising in low-thrust transfers design. As for the equinoctial OEs, Gauss planetary equations are employed in this work to describe the time evolution of MEEs while the mean longitude λ is used interchangeably with L .

*the notation and order introduced in Walker et al. [19] is used here instead of that in [18].

[†] λ, ν here denote the mean longitude and true anomaly not to be confused with the matrix eigenvalues and the Nonlinearity Index of Eq. (8).

4. Alternate Equinoctial Elements

Alternate equinoctial elements were derived from the equinoctial OEs by Horwood et al. [14] substituting a, λ_0 by n, λ where $n = \sqrt{\mu/a^3}$ is the Keplerian mean motion and λ the mean longitude defined in Eq. (44). The other four elements are f, g, h, k as in Eq. (43)[‡]. Alternate equinoctial elements evolve linearly in time under the assumption of unperturbed Keplerian motion (n, f, g, h, k constant and $d\lambda/dt = n$) and nearly linearly in presence of perturbing forces. In the context of orbit UP, these elements will therefore preserve Gaussianity for longer propagation time spans compared to other coordinates sets. In this work, modified Gauss planetary equations that uses n as first coordinate instead of either a or p are employed to describe their evolution over time.

B. DA based Simplified General Perturbations Model

The Simplified General Perturbations (SGP) model series were originally developed by the US Department of Defense (DoD) for space surveillance applications [25]. Five models have been released over the years, namely SGP, SGP4, SDP4, SGP8 and SDP8. Nowadays, SGP4/SDP4 are collectively known as SGP4 theory and commonly used for the propagation of Two-Lines Element Sets (TLEs). SGP4 is used for near-Earth objects (orbital period $< 225 \text{ min}$) and include the effects of Earth's nonuniform gravity field and atmospheric drag. SDP4 is used for deep-space objects (orbital period $\geq 225 \text{ min}$) and adds to SGP4 the contribution of lunisolar perturbations and Earth's resonance terms for geosynchronous and highly-elliptical semi-synchronous orbits. TLEs produced daily by NORAD contain the mean OEs of a space object and other relevant information. These elements are intrinsic to the SGP4 theory and osculating OEs at any epoch must be computed with the relevant SGP4/SDP4 propagator. The lasts are analytical functions that computes an osculating state in cartesian parameters given a TLE and the epoch τ at which the state is sought

$$\mathbf{x}_{TEME}(\tau) = \mathbf{f}_{SGP4}(\tau, TLE) \quad (45)$$

Mean TLE elements and osculating states output of Eq. (45) are expressed in True Equator Mean Equinox (TEME) frame. Since an exact definition of this frame is not available in the literature, it is recommended to convert TEME states into a truly standard coordinate system before interfacing with external routines [25]. Transformations from TEME to Geocentric Celestial Reference Frame (GCRF) are described for example in Vallado [26].

If the computation of \mathbf{x}_{TEME} from a TLE and τ is straightforward and consists in a single function evaluation, the opposite is not true and care must be taken while converting an osculating state into the equivalent TLE representation. Inversion of Eq. (45) can still be accomplished with the iterative procedure summarized in Algorithm 3.

Evaluation of Eq. (45) and Algorithm 3 do not pose any relevant computational issue if performed in Floating Point (FP) arithmetic. Moreover, Eq. (45) contains only algebraic operations that are easily implemented in the DA framework. However, Algorithm 3 cannot be directly applied to Taylor polynomials due to the iterative procedure and associated convergence criterion. In this work, a simple check on the constant part of $[\Delta\mathbf{x}_{kep,osc}^{(i)}]$ is performed to exit the while loop in Algorithm 3. $\|\Delta\mathbf{x}_{kep,osc}^{(i)}\|$ is thus replaced by $\|\overline{\Delta\mathbf{x}}_{kep,osc}^{(i)}\| = \|\mathit{cons}([\Delta\mathbf{x}_{kep,osc}^{(i)}])\|$.

Denoting with $[\mathbf{x}_{TEME}] = \overline{\mathbf{x}}_{TEME} + \boldsymbol{\beta} \cdot \delta\mathbf{x}_{TEME}$ the nominal cartesian state and associated uncertainty, the evaluation of Algorithm 3 on $(\tau, [\mathbf{x}_{TEME}])$ outputs the Taylor expansion of the TLE with respect to deviations in the initial osculating state, i.e. $[TLE] = \mathcal{T}_{TLE}(\delta\mathbf{x}_{TEME})$. The uncertainty in the mean TLE elements is thus obtained directly from $\mathcal{T}_{TLE}(\delta\mathbf{x}_{TEME})$ while a posteriori estimation is required if FP arithmetic is used.

Choosing SGP4 as low-fidelity dynamical model for the multifidelity UP method ultimately relies on its integration within the LOADS-GMM framework described in Section II. A function in the form of Eq. (1) is thus sought in which both \mathbf{x} and \mathbf{y} are osculating orbit states expressed in either one of the OEs sets in Section III.A. A wrapper is then built around Eq. (45) to be used as LOADS target function as summarized in Algorithm 4.

[‡]the notation and order introduced in [19] is used here instead of that in [14].

Algorithm 3 TLE from osculating cartesian state

```
function STATEToTLE( $\tau, \mathbf{x}_{TEME}, \varepsilon_{max}, i_{max}$ )  
  Compute osculating Keplerian elements  $\mathbf{x}_{kep,osc}$  from  $\mathbf{x}_{TEME}$   
  Initialize  $\mathbf{x}_{cart}^{(i)}$  with  $\mathbf{x}_{TEME}$   
  Initialize  $\mathbf{x}_{kep,osc}^{(i)}$  with  $\mathbf{x}_{kep,osc}$   
  Initialize mean elements  $\mathbf{x}_{kep,mean}^{(i)}$  with  $\mathbf{x}_{kep,osc}^{(i)}$   
   $i \leftarrow 0$   
  while  $i < i_{max}$  do  
    Evaluate Eq. (45) in  $\tau, \mathbf{x}_{kep,mean}^{(i)}$  and update  $\mathbf{x}_{cart}^{(i)}$   
    Compute  $\mathbf{x}_{kep,osc}^{(i)}$  from  $\mathbf{x}_{cart}^{(i)}$   
    Compute  $\Delta\mathbf{x}_{kep,osc}^{(i)} = \mathbf{x}_{kep,osc}^{(i)} - \mathbf{x}_{kep,osc}$   
    if  $\|\Delta\mathbf{x}_{kep,osc}^{(i)}\| < \varepsilon_{max}$  then  
      Build the TLE from  $\mathbf{x}_{kep,mean}^{(i)}$   
      break  
    else  
      Compute  $\mathbf{x}_{kep,mean}^{(i)} = \mathbf{x}_{kep,mean}^{(i)} + \Delta\mathbf{x}_{kep,osc}^{(i)}$   
    end if  
     $i \leftarrow i + 1$   
  end while  
  return TLE
```

Algorithm 4 LOADS target function for SGP4 dynamical model

```
function TARGETSGP4( $\tau_0, \tau, [\mathbf{x}_{osc}(\tau_0)]$ )  
  Compute cartesian state  $[\mathbf{x}_{cart}(\tau_0)]$  from  $[\mathbf{x}_{osc}(\tau_0)]$   
  Transform  $[\mathbf{x}_{cart}(\tau_0)]$  into  $[\mathbf{x}_{TEME}(\tau_0)]$  expressed in TEME frame  
  Compute initial TLE from  $[\mathbf{x}_{TEME}(\tau_0)]$  ▷ see Algorithm 3  
  Compute  $[\mathbf{x}_{TEME}(\tau)]$  from initial TLE ▷ see Eq. (45)  
  Transform  $[\mathbf{x}_{TEME}(\tau)]$  into  $[\mathbf{x}_{cart}(\tau)]$  expressed in original frame  
  Compute final state  $[\mathbf{x}_{osc}(\tau)]$  from  $[\mathbf{x}_{cart}(\tau)]$   
  return  $[\mathbf{x}_{osc}(\tau)]$ 
```

C. Multifidelity LOADS-GMM Algorithm

The MF method developed in this work comprises two steps, a low-fidelity (LF) propagation carried out in DA framework and an high-fidelity (HF) one executed point-wise (PW) for a posteriori correction of the LF step.

The SGP4 model described in Section III.B is chosen for the LF dynamics since its analytical formulation allows a straightforward integration with the LOADS-GMM algorithm. An accurate numerical propagator is then used for the HF correction. The overall MF method is detailed in Algorithm 5.

Algorithm 5 Multifidelity orbit Uncertainty Propagation algorithm

function MULTIFIDELITYORBITUP($t_0, t, \boldsymbol{\mu}_X(t_0), \mathbf{P}_X(t_0), c, \alpha_{min}, \varepsilon_v, N_{max}, \mathcal{S}_l$)

Model the initial uncertainty on the orbit state as a multivariate Gaussian distribution

$$p_X(\mathbf{x}(t_0)) \sim \mathcal{N}(\boldsymbol{\mu}_X(t_0), \mathbf{P}_X(t_0)) \quad (46)$$

Initialize $[\mathbf{x}] = [\mathbf{x}_{LF}(t_0)]$ from $\boldsymbol{\mu}_X(t_0), \mathbf{P}_X(t_0)$ ▷ see Eq. (34)Run the LOADS-GMM algorithm with SGP4 as target function f ▷ see Algorithms 2 and 4Approximate the initial PDF $p_X(\mathbf{x}(t_0))$ ▷ see Eq. (38)

$$p_X(\mathbf{x}(t_0)) \simeq \sum_{p=1}^P \alpha^{(p)} p_N(\mathbf{x}; \boldsymbol{\mu}_{LF}^{(p)}(t_0), \mathbf{P}_{LF}^{(p)}(t_0)) \quad (47)$$

Propagate the initial means $\boldsymbol{\mu}_{LF}^{(p)}(t_0)$ in high-fidelity to obtain $\boldsymbol{\mu}_{HF}^{(p)}(t)$ Separate the constant part and nilpotent part of the Taylor expansions $[\mathbf{x}_{LF}^{(p)}(t)]$

$$[\mathbf{x}_{LF}^{(p)}(t)] = \bar{\mathbf{x}}_{LF}^{(p)}(t) + \mathcal{T}_{\delta \mathbf{x}_{LF}^{(p)}(t)}(t_0, \delta \mathbf{x}_0) \quad (48)$$

Substitute $\bar{\mathbf{x}}_{LF}^{(p)}(t)$ in Eq. (48) with $\boldsymbol{\mu}_{HF}^{(p)}(t)$

$$[\mathbf{x}_{MF}^{(p)}(t)] = \boldsymbol{\mu}_{HF}^{(p)}(t) + \mathcal{T}_{\delta \mathbf{x}_{LF}^{(p)}(t)}(t_0, \delta \mathbf{x}_0) \quad (49)$$

Estimate the transformed PDF from $[\mathbf{x}_{MF}^{(p)}(t)]$ ▷ see Eqs. (38) and (41)

$$p_X(\mathbf{x}(t)) \simeq \sum_{p=1}^P \alpha^{(p)} p_N(\mathbf{x}; \boldsymbol{\mu}_{MF}^{(p)}(t), \mathbf{P}_{MF}^{(p)}(t)) \quad (50)$$

return $p_X(\mathbf{x}(t))$

If SGP4 is used as LF dynamical model, the polynomial shift in Eq. (49) might be performed in either osculating or mean TLE elements space. Being $\boldsymbol{\mu}_{HF}^{(p)}(t)$ and $\mathcal{T}_{\delta \mathbf{x}_{LF}^{(p)}(t)}(t_0, \delta \mathbf{x}_0)$ expressed in the chosen osculating coordinates set, a single step is required to apply Eq. (49) in this space. Conversely, intermediate operations are needed to perform this shift in TLE space. The procedure is detailed in Algorithm 6 while its effect on the overall accuracy of the UP method is discussed in Section IV.

Algorithm 6 Polynomial shift in mean TLE elements space

function SHIFTTLE($\boldsymbol{\mu}_{HF}^{(p)}(t), \mathcal{T}_{\delta \mathbf{x}_{LF}^{(p)}(t)}(t_0, \delta \mathbf{x}_0)$)Transform $\boldsymbol{\mu}_{HF}^{(p)}(t), \mathcal{T}_{\delta \mathbf{x}_{LF}^{(p)}(t)}(t_0, \delta \mathbf{x}_0)$ into $\boldsymbol{\mu}_{TEME,HF}^{(p)}(t), \mathcal{T}_{\delta \mathbf{x}_{TEME,LF}^{(p)}(t)}(t_0, \delta \mathbf{x}_0)$ Compute $\boldsymbol{\mu}_{TLE,HF}^{(p)}(t), \mathcal{T}_{\delta \mathbf{x}_{TLE,LF}^{(p)}(t)}(t_0, \delta \mathbf{x}_0)$ from $\boldsymbol{\mu}_{TEME,HF}^{(p)}(t), \mathcal{T}_{\delta \mathbf{x}_{TEME,LF}^{(p)}(t)}(t_0, \delta \mathbf{x}_0)$ ▷ see Algorithm 3Compute $[\mathbf{x}_{TLE,MF}^{(p)}(t)] = \boldsymbol{\mu}_{TLE,HF}^{(p)}(t) + \mathcal{T}_{\delta \mathbf{x}_{TLE,LF}^{(p)}(t)}(t_0, \delta \mathbf{x}_0)$ Compute $[\mathbf{x}_{TEME,MF}^{(p)}(t)]$ from $[\mathbf{x}_{TLE,MF}^{(p)}(t)]$ ▷ see Eq. (45)Transform $[\mathbf{x}_{TEME,MF}^{(p)}(t)]$ into $[\mathbf{x}_{MF}^{(p)}(t)]$ **return** $[\mathbf{x}_{MF}^{(p)}(t)]$

IV. Numerical Results

Three applications of the multifidelity method for orbit Uncertainty Propagation are presented in this section. The analytical SGP4 model is used for the LF dynamics while the HF propagation is carried out numerically taking into account the following force models

- 1) Earth non-uniform gravity field with 8×8 spherical harmonics potential [27]
- 2) Sun and Moon third-body forces with bodies positions from JPL ephemerides
- 3) Isotropic drag force with modified Harris-Priester static atmosphere model [28] (LEO case only)
- 4) Isotropic Solar Radiation Pressure (SRP) force including Earth's umbra and penumbra transitions [29]

The Dormand-Prince 8(5,3) integrator available in Hipparchus[§] is used for the numerical propagation of the high-fidelity ODEs while the Earth potential and atmosphere models are those of Orekit[¶]. All simulations were run with initial epoch set on January 1st, 2021 00:00:00 UTC and force models parameters summarized in Table 2.

Parameter	Value	Description
μ_E	398 600.4355 km ³ s ⁻²	Earth standard gravitational parameter
m	500.0 kg	satellite mass
A_n	1.0 m ²	satellite cross section area
C_D	2.0	atmospheric drag coefficient
C_R	1.5	SRP reflection coefficient

Table 2 Force models parameters

The first two simulations are adapted from [13] and include an High Earth Orbit (HEO) and a Low Earth Orbit (LEO) cases. The last scenario is a Medium Earth Orbit (MEO) orbit for the Galileo constellation. Nominal Initial Conditions (ICs) are summarized in Table 3. The corresponding initial uncertainties are assumed Gaussian with 1σ deviations in cartesian parameters given in Table 4.

Regime	a , km	e	i , deg	Ω , deg	ω , deg	M , deg
HEO	35 000.0	0.2	0.0	0.0	0.0	0.0
LEO	6678.0	0.01	0.0	0.0	0.0	0.0
MEO	29 600.135	0.0	56.0	0.0	0.0	0.0

Table 3 Nominal Initial Conditions for all test cases

Regime	σ_x , km	σ_y , km	σ_z , km	σ_{v_x} , m s ⁻¹	σ_{v_y} , m s ⁻¹	σ_{v_z} , m s ⁻¹
HEO	1.0	1.0	0.0	1.0	1.0	0.0
LEO	1.3	0.5	0.0	2.5	5.0	0.0
MEO	0.5	1.0	1.0	0.5	0.5	0.5

Table 4 Initial uncertainties for all test cases

To better match the bell-shaped Gaussian PDF and minimize the number of new components generated by the LOADS algorithm, the splitting library in Table 1 with $L = 3$ is selected. The Confidence Interval is also set to

[§]<https://hipparchus.org/>

[¶]<https://www.orekit.org/>

$c = 3$. The maximum number of splits and minimum components weight are chosen as $N_{max} = 20$ and $\alpha_{min} = 10^{-8}$ respectively so that the imposed nonlinearity threshold ε_ν is always satisfied. The last is tuned depending on the specific orbit regime and coordinates set as described below.

Keplerian parameters $\bar{\mathbf{x}}_{0,kep}$ in Table 3 are converted to cartesian elements $\bar{\mathbf{x}}_{0,cart}$ and the initial covariance matrix is obtained as $\mathbf{P}_{0,cart} = \text{diag}(\sigma_{0,cart}^2)$ with $\sigma_{0,cart}$ given by Table 4. The corresponding DA state $[\mathbf{x}_{0,cart}]$ is then initialized according to Eq. (34). For simulations carried out in OEs other than cartesian parameters, $[\mathbf{x}_{0,cart}]$ must be converted to an IC in the corresponding elements set. This is achieved with Algorithm 2 choosing \mathbf{f} as the coordinate transformation from cartesian to target OEs and a nonlinearity threshold $\varepsilon_\nu = 0.01$. For all proposed scenarios, a single Gaussian kernel is sufficient for this map. Each resulting IC is then propagated for two Keplerian periods of the corresponding nominal orbit.

A. Uncertainty Propagation in Cartesian Parameters

A first qualitative analysis on the orbit UP algorithm in cartesian parameters is conducted in this section. Iso-probability lines of the propagated state PDF and reference MC samples are plotted in Sections IV.A.1 to IV.A.3 to visually assess the accuracy of the proposed UP method. A quantitative measure of the accuracy of the proposed multifidelity method is provided in Section IV.C.

1. High Earth Orbit

Output of the HEO case obtained with $\varepsilon_\nu = 0.01$ are displayed in Fig. 1. Figure 1a shows a projection of the propagated uncertainty in position onto the $x - y$ plane while Fig. 1b represents the uncertainty in velocity on the same plane. Values of the estimated PDF are normalized with respect to their maximum located in correspondence of the nominal solution. The final GMM includes 6561 components to accurately represent the strongly non-Gaussian PDF as demonstrated by the contour lines following the curvature of the reference MC samples.

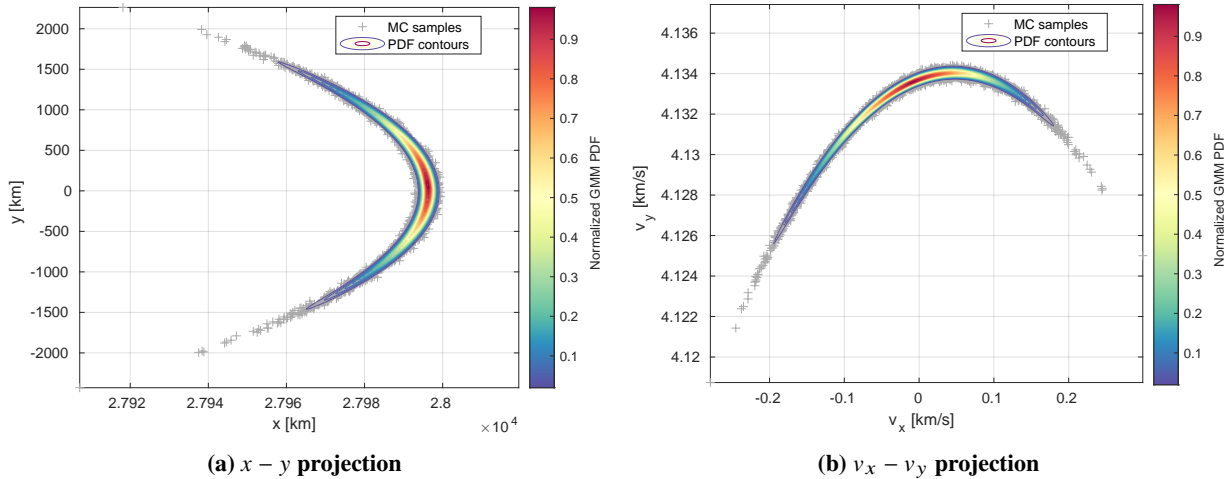


Fig. 1 Propagated MC samples and mixture PDF in cartesian parameters for High Earth Orbit case

2. Low Earth Orbit

The second scenario is the equatorial LEO orbit for which the estimated PDF is displayed in Fig. 2. Figure 2a shows a projection of the uncertainty in position onto the $x - y$ plane while Fig. 2b a projection of the corresponding uncertainty in velocity onto the same plane. As before, the effects of nonlinearity are visible in the curvature of the initially Gaussian MC samples set, closely followed by the contour lines of the estimated PDF. Despite the higher nonlinearity threshold $\varepsilon_\nu = 0.025$ and the lower eccentricity with respect to the previous case, 2187 kernels are needed to approximate the transformed PDF mainly due to the lower orbit altitude and the consequent atmospheric drag.

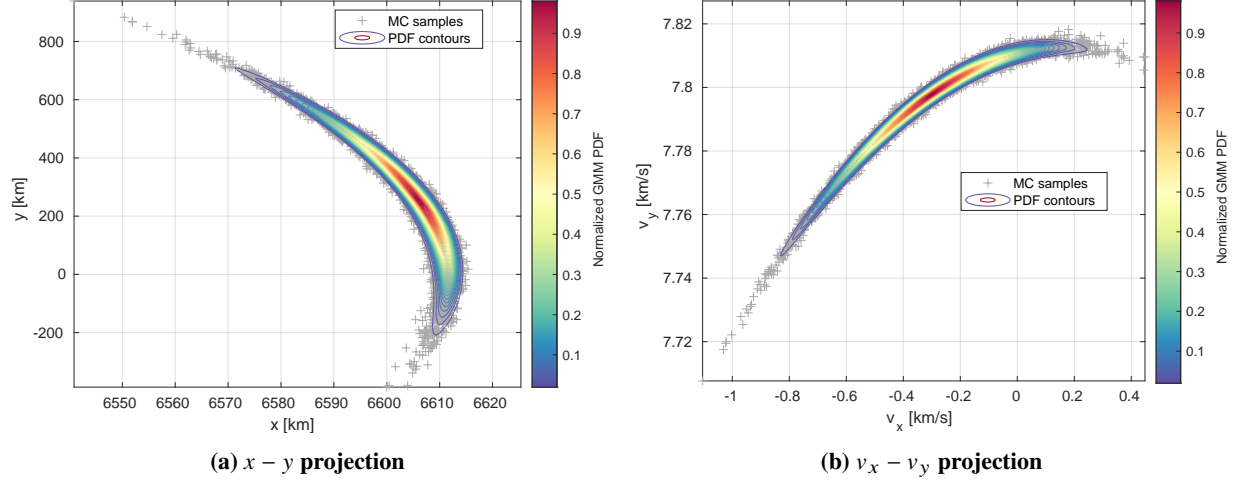


Fig. 2 Propagated MC samples and mixture PDF in cartesian parameters for Low Earth Orbit case

3. Medium Earth Orbit

The last test case is the circular, inclined orbit of the Galileo constellation. The propagated uncertainties are shown in Fig. 3 together with the reference MC samples. Figure 3a represents the uncertainty in position projected on the $x - z$ plane while Fig. 3b the corresponding uncertainty in velocity. In this case, setting $\varepsilon_v = 0.01$ leads to 729 GMM components required to approximate the propagated PDF. The great reduction in the number of kernels with respect to the previous cases is mainly due to the lower eccentricity (compared to the HEO case), the longer orbital period and the absence of atmospheric drag (compared to the LEO case). The lower number of components is thus a hint of the weaker nonlinearity of the dynamics in this scenario as demonstrated by the shape of the contour lines in Fig. 3b. This behavior also highlights the advantages of an adaptive splitting scheme with respect to more conventional GMMs with fixed number of components: the final number of Gaussian kernels is guaranteed to be the minimum required to satisfy the imposed nonlinearity threshold.

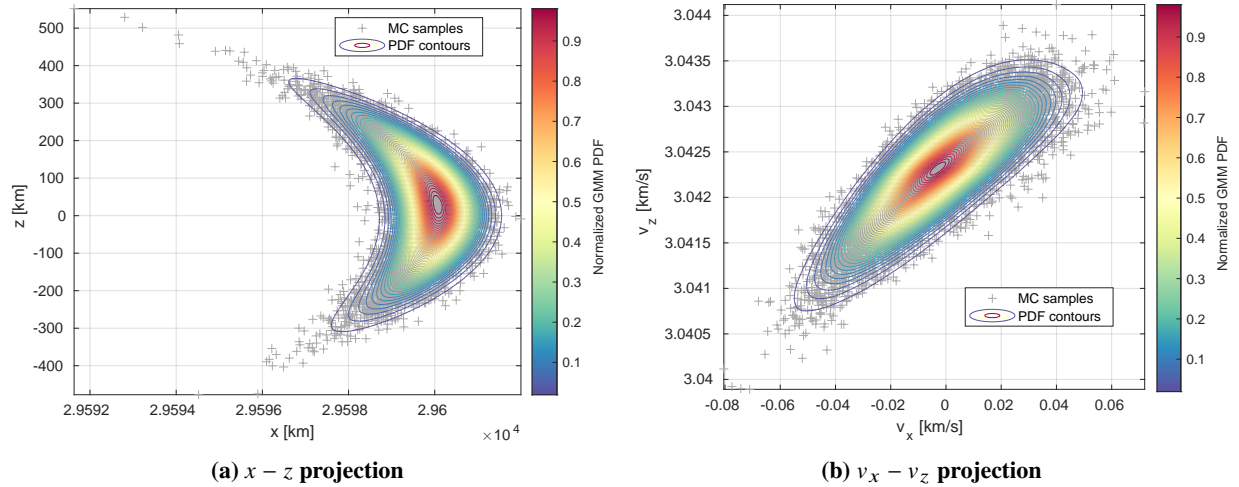


Fig. 3 Propagated MC samples and mixture PDF in cartesian parameters for Medium Earth Orbit case

B. Sensitivity to State Parametrization and LOADS-GMM Parameters

1. Sensitivity to State Parametrization

This section discusses the impact of the state parametrization, i.e. the selected coordinates set, on the overall MF algorithm. Twenty-one simulations were carried out. They correspond to all possible combinations among orbit regime (i.e. HEO/LEO/MEO), coordinates set (i.e. cartesian/equinoctial/MEE/alternate elements) and position angles (i.e. L , λ , not applicable for cartesian parameters). For each case, the imposed nonlinearity threshold ε_ν , final number of Gaussian kernels N_f and single-domain NLI ν_s are reported in Table 5. ν_s corresponds to the NLI of the final domain $[x(t)]$ when mapped without ADS and a direct measure of nonlinearity of the different representations. For a fixed threshold ε_ν , ν_s is thus expected to be directly correlated with the final number of components N_f . This fact is demonstrated in Fig. 4 in which N_f is plotted as function of the normalized single-domain NLI ν_s/ε_ν (only the cases for which $\nu_s > \varepsilon_\nu$ and thus $N_f > 1$ are shown in the picture). For each orbit regime, the number of components decreases monotonically for decreasing ν_s/ε_ν as expected by construction of the LOADS algorithm.

OEs	High Earth Orbit			Low Earth Orbit			Medium Earth Orbit			
	ν_s	ε_ν	N_f	ν_s	ε_ν	N_f	ν_s	ε_ν	N_f	
Cartesian	–	7.121×10^{-2}	0.01	6561	1.096×10^{-1}	0.025	2187	2.709×10^{-2}	0.01	729
Equinoctial	L	1.343×10^{-2}	0.003	3115	2.518×10^{-2}	0.01	277	4.067×10^{-3}	0.003	9
MEEs	L	1.195×10^{-2}	0.003	2187	3.145×10^{-2}	0.01	2221	5.946×10^{-3}	0.003	243
Alternate	L	8.210×10^{-3}	0.003	729	1.927×10^{-2}	0.01	93	2.797×10^{-3}	0.003	1
Equinoctial	λ	4.342×10^{-3}	0.003	3	1.170×10^{-2}	0.01	3	1.576×10^{-3}	0.003	1
MEEs	λ	6.982×10^{-3}	0.003	729	1.798×10^{-2}	0.01	83	3.457×10^{-3}	0.003	3
Alternate	λ	7.151×10^{-6}	0.003	1	3.783×10^{-3}	0.01	1	1.737×10^{-5}	0.003	1

Table 5 Single-domain NLI ν_s , nonlinearity threshold ε_ν and number of GMM components for all tests cases

From Table 5 it is clear that cartesian parameters are the most nonlinear since they lead to larger number of kernels despite the higher thresholds selected in this case. Moreover, the use of alternate elements and mean longitude λ results in a quasi-linear transformation that is correctly captured by a single polynomial as seen in the last row of Table 5.

Unfortunately, coordinates sets can rarely be chosen freely. Many applications such as collision probability estimation require the state uncertainty at the Time of Closest Approach (TCA) expressed in cartesian parameters. Adding a coordinate transformation at the end of the LOADS target function f will be detrimental in this case since the NLI will still be computed on cartesian parameters, thus losing all benefits of alternative state parametrizations. However, this is only true for analytical propagators such as SGP4 which require a single function evaluation to compute the final state. Conversely, for numerical propagators splits are allowed at any time along the trajectory. Since each split will then correspond to $L - 1$ new trajectories to be propagated[‡], it is of great interest to delay as much as possible these splits and propagate a single expansion for the entire time span. This behavior could be achieved using alternate equinoctial elements for the propagation itself followed by a coordinate transformation of the single final state in which all splits will occur.

2. Sensitivity to Minimum Kernel Weight

Since the number of GMM components output of the MF method are bounded by the maximum allowed number of splits N_{max} and the minimum kernel weight α_{min} , it is of interest to analyze the impact of α_{min} on the accuracy of the estimated PDF. This analysis is conducted in cartesian parameters since this coordinates set generates the highest number of splits and is thus the one which is penalized the most by large thresholds on α_{min} . For the three test cases presented above, multiple solutions were obtained for different values of $\alpha_{min} \in [1, 10^{-8}]$ and the corresponding LAM with respect to the same set of MC samples computed using Eq. (33). These values were then normalized with respect to the solution with the highest allowed number of kernels, i.e.

[‡]details on how numerical integrators can be embedded in the LOADS framework are provided in [12]

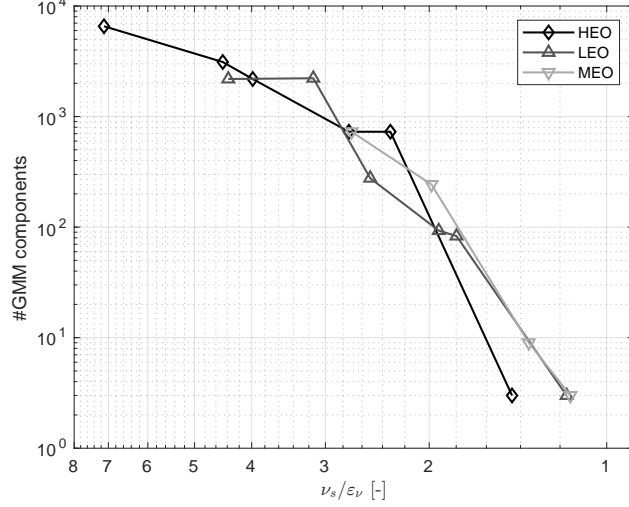


Fig. 4 Number of GMM components as function of normalized single-domain NLI ν_s/ε_ν

$$\mathcal{L}_{n,MF}(\alpha_{min}) = \frac{\mathcal{L}_{MF}(\alpha_{min})}{\mathcal{L}_{MF}(\alpha_{min})|_{\alpha_{min}=10^{-8}}} \quad (51)$$

The final number of components N_f and normalized LAM \mathcal{L}_n are shown in Fig. 5 as a function of α_{min} .

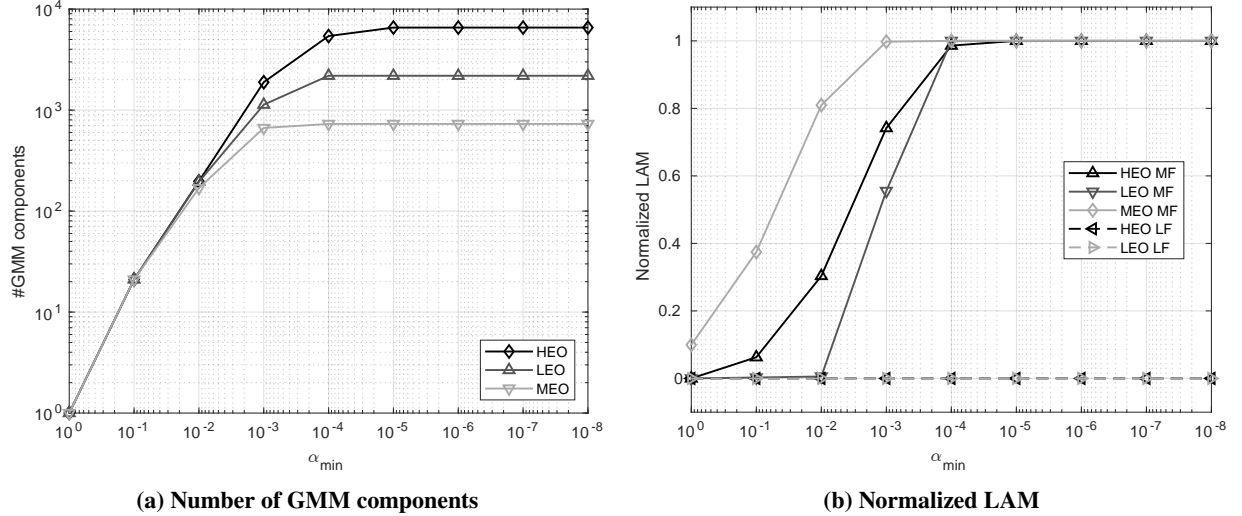


Fig. 5 Number of GMM components and normalized LAM as function of α_{min}

As can be seen in Fig. 5a, for the High Earth Orbit test case no more than 6561 kernels with $\alpha_i > 10^{-5} \forall i$ are needed to satisfy the imposed nonlinearity threshold ε_ν . For $\alpha_{min} < 10^{-5}$ a plateau is in fact reached in both figures, thus signifying the same PDF estimation is obtained for smaller values. On the contrary, looking at Fig. 5b from right to left a rapid decrease in \mathcal{L}_n is observed for $\alpha_{min} \rightarrow 1$, i.e. for a number of GMM components that is progressively reduced to a single Gaussian kernel. Similar conclusions can be drawn for the LEO and MEO cases in which the plateau is reached for $\alpha_{min} = 10^{-4}$ corresponding to 2187 and 729 components respectively. These results demonstrate the flexibility and accuracy of the proposed MF approach which eliminates the needs of a priori estimation of the required number of kernels to guarantee a certain accuracy thus minimizing the computational effort given the nonlinearity content of the problem at hand.

C. Accuracy of the Multifidelity Method

The Root Mean Square Error (RMSE) is introduced in this section to quantify the error made by the multifidelity method with respect to a reference MC simulation. The RMSE is defined as

$$e_{RMSE} = \sqrt{\frac{1}{N} \sum_{i=1}^N (\mathbf{x}_i - \hat{\mathbf{x}}_i)^2} \quad (52)$$

with $\{\mathbf{x}_i\}$, $\{\hat{\mathbf{x}}_i\}$ expected and actual samples respectively. Note that all operations in Eq. (52) are carried out element-wise so that e_{RMSE} has the same dimension of $\hat{\mathbf{x}}_i, \mathbf{x}_i \forall i$.

To compute $\{\mathbf{x}_n\}$, $\{\hat{\mathbf{x}}_i\}$ in the case of orbit UP, N random samples $\{\mathbf{x}_i(t_0)\}$ are firstly drawn from the initial distribution $p_{\mathbf{X}}(\mathbf{x}(t_0))$ in Eq. (46). $\{\mathbf{x}_i\}$ is then simply obtained with a point-wise propagation of $\{\mathbf{x}_i(t_0)\}$ in HF dynamics. Conversely, $\{\hat{\mathbf{x}}_i\}$ is computed evaluating the Taylor polynomials $[\mathbf{x}_{MF}^{(p)}(t)]$ in $\{\mathbf{x}_i(t_0)\}$ thus avoiding the needs for additional propagation steps. For each entry in Table 5, three samples sets are computed. They correspond to the LF solution and the two multifidelity ones obtained with a polynomial shift applied in either osculating or TLE elements space using Eq. (49) or Algorithm 6 respectively. For the shake of clarity, only a subset of the computed errors is reported in Table 6.

		$x, \text{ km}$	$y, \text{ km}$	$z, \text{ km}$	$v_x, \text{ km s}^{-1}$	$v_y, \text{ km s}^{-1}$	$v_z, \text{ km s}^{-1}$
	LF	8.363×10^{-1}	2.293×10^1	4.155×10^{-1}	2.839×10^{-3}	1.022×10^{-4}	9.126×10^{-5}
	MF _{osc}	2.425×10^{-2}	7.855×10^{-3}	6.657×10^{-4}	8.804×10^{-7}	3.617×10^{-6}	1.344×10^{-7}
HEO	MF _{TLE}	6.977×10^{-4}	9.345×10^{-3}	3.792×10^{-4}	9.771×10^{-7}	1.891×10^{-6}	1.009×10^{-7}
		$a, \text{ km}$	f	g	h	k	$L, \text{ rad}$
	LF	5.766×10^{-2}	2.109×10^{-5}	5.028×10^{-6}	1.108×10^{-5}	7.378×10^{-6}	8.193×10^{-4}
	MF _{osc}	5.386×10^{-4}	1.926×10^{-8}	3.087×10^{-8}	1.180×10^{-8}	6.615×10^{-9}	1.216×10^{-6}
	MF _{TLE}	4.804×10^{-2}	1.098×10^{-6}	5.842×10^{-8}	1.228×10^{-8}	6.570×10^{-9}	1.042×10^{-6}
		$p, \text{ km}$	f	g	h	k	$L, \text{ rad}$
	LF	3.079×10^{-2}	2.956×10^{-5}	2.814×10^{-5}	1.241×10^{-5}	4.622×10^{-6}	4.175×10^{-4}
	MF _{osc}	5.096×10^{-4}	5.828×10^{-8}	1.409×10^{-7}	8.101×10^{-9}	1.661×10^{-9}	7.073×10^{-6}
LEO	MF _{TLE}	6.078×10^{-3}	1.442×10^{-6}	1.143×10^{-6}	8.123×10^{-9}	1.642×10^{-9}	8.429×10^{-6}
		$n, \text{ rad s}^{-1}$	f	g	h	k	$\lambda, \text{ rad}$
	LF	8.956×10^{-9}	2.953×10^{-5}	2.813×10^{-5}	1.241×10^{-5}	4.621×10^{-6}	4.624×10^{-4}
	MF _{osc}	6.898×10^{-10}	2.947×10^{-7}	1.068×10^{-6}	1.625×10^{-7}	2.903×10^{-8}	7.524×10^{-5}
	MF _{TLE}	1.524×10^{-9}	1.410×10^{-6}	4.132×10^{-6}	1.630×10^{-7}	2.845×10^{-8}	7.525×10^{-5}
		$x, \text{ km}$	$y, \text{ km}$	$z, \text{ km}$	$v_x, \text{ km s}^{-1}$	$v_y, \text{ km s}^{-1}$	$v_z, \text{ km s}^{-1}$
	LF	3.157×10^{-2}	1.898	2.800	4.197×10^{-4}	2.797×10^{-6}	1.154×10^{-5}
	MF _{osc}	2.743×10^{-3}	5.512×10^{-4}	8.137×10^{-4}	1.307×10^{-7}	1.658×10^{-7}	2.534×10^{-7}
MEO	MF _{TLE}	5.089×10^{-2}	3.183×10^{-2}	4.725×10^{-2}	3.561×10^{-6}	3.692×10^{-6}	5.470×10^{-6}
		$n, \text{ rad s}^{-1}$	f	g	h	k	$L, \text{ rad}$
	LF	7.115×10^{-10}	4.800×10^{-6}	8.645×10^{-8}	7.066×10^{-7}	1.769×10^{-7}	1.144×10^{-4}
	MF _{osc}	1.772×10^{-11}	9.860×10^{-8}	1.439×10^{-8}	7.864×10^{-9}	1.054×10^{-8}	3.976×10^{-7}
	MF _{TLE}	1.706×10^{-10}	3.337×10^{-6}	6.407×10^{-6}	7.836×10^{-9}	1.049×10^{-8}	1.326×10^{-5}

Table 6 RMSE error for various test cases

Data in Table 6 demonstrate the accuracy of the proposed UP algorithm in terms of both absolute RMSE with respect to the reference MC simulation and relative error with respect to the LF counterpart. When using cartesian

parameters, the absolute RMSE in position is always below 10 m, while the errors in semimajor axis a and semilatus rectum p are smaller than 1 m if the true longitude L is used and below 10 m otherwise. RMSEs in f, g, h, k are below 1×10^{-6} for all types of OEs with MEEs performing best if combined with L . Finally, errors in mean and true longitudes λ, L exhibit a stronger dependence on the orbit regime, with RMSEs that vary from 1×10^{-5} rad in LEO to 1×10^{-7} rad in MEO. The multifidelity correction is key to achieve such small errors since it guarantees a major improvement over the LF solution. In particular, the RMSE is reduced by up to four Orders of Magnitude (OOMs) for propagations in cartesian parameters, with the polynomial shift better performed in osculating elements space. The only exception is the x coordinate in HEO regime, for which a shift in TLE space further reduces the RMSE by two OOMs. Concerning the semimajor axis a , semilatus rectum p and mean motion n , a shift in osculating elements space is always preferred while the application of Algorithm 6 could result in RMSEs close to the LF solution. This behavior is more marked in HEO and MEO regimes. Similar arguments apply to f for which a direct shift results in a two OOMs improvement with respect to the LF baseline. Application of Algorithm 6 results in only one OOM improvement for the HEO and LEO cases and no improvement in MEO. For the g coordinate, the RMSE of the multifidelity solution is one to two OOMs smaller than that of the LF counterpart if the shift is performed in osculating elements space. Conversely, the accuracy is similar in HEO while it degrades in LEO and especially in MEO for shifts in TLE space. Contrarily to the previous cases, the accuracy in h, k does not depend on the space in which the shift is performed and both multifidelity solutions guarantee a two to three OOMs improvement with respect to the LF one. The same behavior is observed for the mean longitude λ and the true longitude L excluding the MEO regime for the last. In this case, the error is one to three OOMs smaller after the correction is applied. Finally, application of Algorithm 6 in MEO regime worsens the RMSE of the LF solution while a three OOMs improvement is otherwise obtained. To summarize, the accuracy of the proposed multifidelity UP method is within few meters in position over a wide range of orbit regimes. Moreover, a simple polynomial shift applied in osculating elements space through Eq. (49) is preferred to Algorithm 6 since the last could result in virtually no improvements over the baseline LF solution.

D. Computational Savings

The MF method presented in this paper has been introduced as an accurate and computationally efficient alternative to more conventional HF approaches for orbit UP. In this section, the computational load of the proposed method is compared to that of an equivalent HF solution. For this purpose, a DA version of the HF numerical propagator is used with the combined LOADS-GMM algorithm to propagate the initial uncertainty directly in HF thus avoiding the needs for a posteriori correction¹. All numerical simulations were run on an Intel Core i5-9400H @ 2.50 GHz with 16GB of RAM running Ubuntu 18.04 LTS. The total runtime was approximated from that of a single propagation as

$$T_{MF} \approx L \cdot (t_{DA,LF} + t_{PW,HF}) \quad (53a)$$

$$T_{HF} \approx L \cdot t_{DA,HF} \quad (53b)$$

where L is the number of Gaussian kernels and the subscripts DA and PW indicate whether the propagation is performed in DA or point-wise. The runtimes for single kernels in cartesian parameters are summarized in Table 7.

Regime	$t_{DA,LF}$, ms	$t_{PW,HF}$, ms	t_{MF} , ms	$t_{DA,HF}$, ms	$t_{DA,HF}/t_{MF}$, -
HEO	2.805	67.395	70.200	1442.065	20.542
LEO	1.855	353.120	354.975	5389.915	15.184
MEO	2.350	60.560	62.910	1176.670	18.704

Table 7 Runtime for a single propagation in cartesian parameters for all test cases

As seen in Table 7, the MF method is 15 to 20 times faster than the HF counterpart with the High Earth Orbit case providing the highest speedup. Moreover, within the MF procedure most of the time is spent in the correction step which must be carried out numerically for maximum accuracy. This fact is more marked for the LEO case where the low orbit altitude and the presence of atmospheric drag further slow down the numerical integration.

V. Conclusions

A novel multifidelity method for Uncertainty Propagation is presented. The approach leverages Differential Algebra techniques and Gaussian Mixture Models to efficiently map the initial uncertainties through arbitrary nonlinear transformations. A DA-based measure of nonlinearity is computed to detect departure from linearity of each kernel and a splitting algorithm is employed to adapt on demand the number of GMM components needed to satisfy the desired accuracy. Second-order Taylor expansions of the function output with respect to the initial uncertainty are then used to efficiently map the initial statistics using Unscented Transform sigma points. The combined LOADS-GMM algorithm is run on a LF model to minimize the associated computational load. A high-fidelity propagation of the kernels centers is inserted before the UT sampling to improve the accuracy of the low-fidelity maps. The MF algorithm is then applied to the problem of orbit UP and three test cases are provided to cover the high-, medium- and low- Earth orbit regimes. The estimated PDFs are compared with reference Monte Carlo simulations and a good agreement between MC samples and PDF contour lines is obtained. The advantages of an adaptive split scheme for the determination of the optimal number of kernels are then highlighted comparing solutions obtained for increasing number of GMM components and the importance of the HF correction is assessed comparing the agreement to MC samples of the LF and MF solutions. The proposed MF approach is estimated to bring a speedup of 15-20 times with respect to its HF counterpart for the same overall accuracy.

Acknowledgments

This work is co-funded by the CNES through A. Fossà's PhD program, and made use of the CNES orbital propagation tools, including the PACE library.

References

- [1] Luo, Y.-z., and Yang, Z., "A review of uncertainty propagation in orbital mechanics," *Progress in Aerospace Sciences*, Vol. 89, 2017, pp. 23–39. <https://doi.org/10.1016/j.paerosci.2016.12.002>.
- [2] Park, R. S., and Scheeres, D. J., "Nonlinear Mapping of Gaussian Statistics: Theory and Applications to Spacecraft Trajectory Design," *Journal of Guidance, Control, and Dynamics*, Vol. 29, No. 6, 2006, pp. 1367–1375. <https://doi.org/10.2514/1.20177>.
- [3] Julier, S., and Uhlmann, J., "Unscented Filtering and Nonlinear Estimation," *Proceedings of the IEEE*, Vol. 92, No. 3, 2004, pp. 401–422. <https://doi.org/10.1109/JPROC.2003.823141>.
- [4] Adurthi, N., and Singla, P., "Conjugate Unscented Transformation-Based Approach for Accurate Conjunction Analysis," *Journal of Guidance, Control, and Dynamics*, Vol. 38, No. 9, 2015, pp. 1642–1658. <https://doi.org/10.2514/1.G001027>.
- [5] Adurthi, N., Singla, P., and Singh, T., "Conjugate Unscented Transformation: Applications to Estimation and Control," *Journal of Dynamic Systems, Measurement, and Control*, Vol. 140, No. 3, 2018. <https://doi.org/10.1115/1.4037783>.
- [6] Jones, B. A., and Weisman, R., "Multi-fidelity orbit uncertainty propagation," *Acta Astronautica*, Vol. 155, 2019, pp. 406–417. <https://doi.org/10.1016/j.actaastro.2018.10.023>.
- [7] Peherstorfer, B., Willcox, K., and Gunzburger, M., "Survey of Multifidelity Methods in Uncertainty Propagation, Inference, and Optimization," *SIAM Review*, Vol. 60, No. 3, 2018, pp. 550–591. <https://doi.org/10.1137/16M1082469>.
- [8] Berz, M., *Modern Map Methods in Particle Beam Physics*, Academic Press, London, 1999. URL <http://bt.pa.msu.edu/cgi-bin/display.pl?name=AIEP108book>.
- [9] Valli, M., Armellin, R., Di Lizia, P., and Lavagna, M. R., "Nonlinear mapping of uncertainties in celestial mechanics," *Journal of Guidance, Control, and Dynamics*, Vol. 36, No. 1, 2013, pp. 48–63. <https://doi.org/10.2514/1.58068>.
- [10] Armellin, R., and Di Lizia, P., "Probabilistic Optical and Radar Initial Orbit Determination," *Journal of Guidance, Control, and Dynamics*, Vol. 41, No. 1, 2018, pp. 101–118. <https://doi.org/10.2514/1.G002217>.
- [11] Wittig, A., Di Lizia, P., Armellin, R., Makino, K., Bernelli-Zazzera, F., and Berz, M., "Propagation of large uncertainty sets in orbital dynamics by automatic domain splitting," *Celestial Mechanics and Dynamical Astronomy*, Vol. 122, No. 3, 2015, pp. 239–261. <https://doi.org/10.1007/s10569-015-9618-3>.
- [12] Losacco, M., Armellin, R., and Fossà, A., "A low-order automatic domain splitting approach for nonlinear uncertainty mapping," *Journal of Guidance, Control, and Dynamics*, 2021. (not yet published).

- [13] DeMars, K. J., Bishop, R. H., and Jah, M. K., “Entropy-Based Approach for Uncertainty Propagation of Nonlinear Dynamical Systems,” *Journal of Guidance, Control, and Dynamics*, Vol. 36, No. 4, 2013, pp. 1047–1057. <https://doi.org/10.2514/1.58987>.
- [14] Horwood, J. T., Aragon, N. D., and Poore, A. B., “Gaussian Sum Filters for Space Surveillance: Theory and Simulations,” *Journal of Guidance, Control, and Dynamics*, Vol. 34, No. 6, 2011, pp. 1839–1851. <https://doi.org/10.2514/1.53793>.
- [15] Vittaldev, V., Russell, R. P., and Linares, R., “Spacecraft Uncertainty Propagation Using Gaussian Mixture Models and Polynomial Chaos Expansions,” *Journal of Guidance, Control, and Dynamics*, Vol. 39, No. 12, 2016, pp. 2615–2626. <https://doi.org/10.2514/1.G001571>.
- [16] Sun, Z.-J., Luo, Y.-Z., di Lizia, P., and Zazzera, F. B., “Nonlinear orbital uncertainty propagation with differential algebra and Gaussian mixture model,” *Science China Physics, Mechanics & Astronomy*, Vol. 62, No. 3, 2019, p. 34511. <https://doi.org/10.1007/s11433-018-9267-6>.
- [17] Junkins, J. L., and Singla, P., “How Nonlinear Is It? A Tutorial on Nonlinearity of Orbit and Attitude Dynamics,” *The Journal of the Astronautical Sciences*, Vol. 52, No. 1-2, 2004, pp. 7–60. <https://doi.org/10.1007/BF03546420>.
- [18] Broucke, R. A., and Cefola, P. J., “On the equinoctial orbit elements,” *Celestial Mechanics*, Vol. 5, No. 3, 1972, pp. 303–310. <https://doi.org/10.1007/BF01228432>.
- [19] Walker, M. J. H., Ireland, B., and Owens, J., “A set modified equinoctial orbit elements,” *Celestial Mechanics*, Vol. 36, No. 4, 1985, pp. 409–419. <https://doi.org/10.1007/BF01227493>.
- [20] Aristoff, J. M., Horwood, J. T., and Alfriend, K. T., “On a set of J_2 equinoctial orbital elements and their use for uncertainty propagation,” *Celestial Mechanics and Dynamical Astronomy*, Vol. 133, No. 9, 2021, p. 19. <https://doi.org/10.1007/s10569-021-10004-0>.
- [21] Baù, G., Hernando-Ayuso, J., and Bombardelli, C., “A generalization of the equinoctial orbital elements,” *Celestial Mechanics and Dynamical Astronomy*, Vol. 133, No. 50, 2021, p. 29. <https://doi.org/10.1007/s10569-021-10049-1>.
- [22] Wächter, A., and Biegler, L. T., “On the implementation of an interior-point filter line-search algorithm for large-scale nonlinear programming,” *Mathematical Programming*, Vol. 106, No. 1, 2006, pp. 25–57. <https://doi.org/10.1007/s10107-004-0559-y>.
- [23] “HSL. A collection of Fortran codes for large scale scientific computation.”, 2021. URL <http://www.hsl.rl.ac.uk/>.
- [24] Battin, R. H., *An Introduction to the Mathematics and Methods of Astrodynamics, Revised Edition*, American Institute of Aeronautics and Astronautics, Reston, VA, 1999. <https://doi.org/10.2514/4.861543>.
- [25] Vallado, D. A., Crawford, P., Hujsak, R., and Kelso, T., “Revisiting Spacetrack Report #3,” *AIAA/AAS Astrodynamics Specialist Conference and Exhibit*, American Institute of Aeronautics and Astronautics, Keystone, Colorado, 2006, pp. 1–88. <https://doi.org/10.2514/6.2006-6753>.
- [26] Vallado, D. A., *Fundamentals of Astrodynamics and Applications*, 4th ed., Microcosm Press, Hawthorne, CA, 2013.
- [27] Holmes, S. A., and Featherstone, W. E., “A unified approach to the Clenshaw summation and the recursive computation of very high degree and order normalised associated Legendre functions,” *Journal of Geodesy*, Vol. 76, No. 5, 2002, pp. 279–299. <https://doi.org/10.1007/s00190-002-0216-2>.
- [28] Harris, I., and Priester, W., “Time-Dependent Structure of the Upper Atmosphere,” *Journal of the Atmospheric Sciences*, Vol. 19, No. 4, 1962, pp. 286–301. [https://doi.org/10.1175/1520-0469\(1962\)019<0286:TDSOTU>2.0.CO;2](https://doi.org/10.1175/1520-0469(1962)019<0286:TDSOTU>2.0.CO;2).
- [29] Hubaux, C., Lemaître, A., Delsate, N., and Carletti, T., “Symplectic integration of space debris motion considering several Earth’s shadowing models,” *Advances in Space Research*, Vol. 49, No. 10, 2012, pp. 1472–1486. <https://doi.org/10.1016/j.asr.2012.02.009>.